Journal of Materials Chemistry A

Improved Synthesis and Transient Absorption Spectroscopy of $CuBiW_2O_8$ with Demonstration of Visible-Light-Driven Photocatalysis and Mechanistic Insights

Journal:	*Journal of Materials Chemistry A*
Manuscript ID	TA-ART-04-2022-003086.R2
Article Type:	Paper
Date Submitted by the Author:	03-Oct-2022

Complete List of Authors:	Yilmaz Akkaya, Ceren; Worcester Polytechnic Institute, Mechanical Engineering Dombrowski, James; Worcester Polytechnic Institute, Mechanical Engineering Colin-Ulloa, Erika; Worcester Polytechnic Institute, Physics Titova, Lyubov; Worcester Polytechnic Institute, Lawton, Timothy; Natick Soldier Research Development and Engineering Center, Soldier Protection Directorate, US Army Combat Capabilities Development Command Soldier Center Alexander, Todd; Natick Soldier Research Development and Engineering Center, Soldier Protection Directorate, US Army Combat Capabilities Development Command Soldier Center Brack, Eric; Natick Soldier Research Development and Engineering Center, Soldier Protection Directorate, US Army Combat Capabilities Development Command Soldier Center Drew, Christopher; Natick Soldier Research Development and Engineering Center, Soldier Protection Directorate, US Army Combat Capabilities Development Command Soldier Center Rao, Pratap; Worcester Polytechnic Institute, Mechanical Engineering

ARTICLE

Improved Synthesis and Transient Absorption Spectroscopy of $CuBiW_2O_8$ with Demonstration of Visible-Light-Driven Photocatalysis and Mechanistic Insights

Received 00th January 20xx,
Accepted 00th January 20xx

DOI: 10.1039/x0xx00000x

Ceren Yilmaz Akkaya[a], James Dombrowski,[a] Erika Colin-Ulloa,[b] Lyubov V. Titova,[b] Timothy J. Lawton,[c] Todd Alexander,[c] Eric Brack,[c] Christopher Drew,[c] Pratap M. Rao[a,*]

$CuBiW_2O_8$ (CBTO), with a band gap of 1.9-2.0 eV, responds to a wide region of the electromagnetic spectrum, which makes it a good candidate for solar-driven photocatalytic energy conversion and water treatment. We have previously demonstrated a Cu-rich solid state approach that enables the synthesis of CBTO accompanied by thermodynamically stable Bi_2WO_6 impurity. Here, we describe an improved synthesis protocol with decreased impurity and synthesis time, and the first demonstration of CBTO as a functional material using photocatalytic Cr(VI) photoreduction as a probe reaction. Transient absorption spectroscopy (TAS) was performed to investigate the ultrafast dynamics of the charge carriers after photoexcitation. The presence of two populations of photoexcited carriers was found, including short-lived free carriers with ~10 ps lifetime and long-lived shallowly-trapped carriers with ~1 ns lifetime. Together with carrier mobilites measured in our previous study, the new TAS results indicate that the long-lived charges have diffusion lengths similar to the CBTO particle size and were likely responsible for the majority of the photocatalytic activity. High activity of CBTO for Cr(VI) photoreduction (~100% reduction of 5 mg/L of Cr(VI) in 15 minutes) was demonstrated, which clearly establishes the promise of this novel oxide for visible light-driven photocatalytic applications. Radical quenching experiments indicate that both $^{\bullet}OH$ radicals and $O_2^{\bullet -}$ radicals are produced by CBTO and are involved in the photoreduction of Cr(VI). Repeated photocatalysis tests and analysis of the surface after the reaction show that CBTO is a stable and potentially reusable catalyst. Insights gained from correlating the synthesis conditions, carrier dynamics, and reactive species suggests that CBTO prepared with the improved protocol would be a favorable choice for photocatalytic reactions such as water decontamination from organic pollutants, water splitting, and solar fuel generation using visible light.

1. Introduction

Copper-containing complex oxides are promising candidates for light-driven catalysis such as photocatalytic pollutant removal/degradation and photoelectrochemical water splitting.[1–10] Development of sustainable catalysts with strong optical absorption in the visible range is important for efficient energy conversion and environmental remediation.

We have previously shown that the quaternary complex oxide, $CuBiW_2O_8$ (CBTO), is a good solar absorber material (absorption coefficient of 10^4 cm^{-1} for 700 nm light) with moderate charge transport[2], which makes CBTO a favourable catalyst for visible-light-induced reactions. However, due to the complexity of the material, studies on CBTO are scarce. Besides, CBTO synthesis is challenging in terms of maintaining Cu in the +1-oxidation state and preventing Cu loss by diffusion during the growth. In our earlier work, we mitigated these challenges by repeating the solid-state synthesis several times within a sealed copper box at 600 °C[2] which is a slightly modified version of the procedure described by Klevtsov and Perepelitsa.[11] However, even after the repeated thermal annealing steps, persistent Bi_2WO_6 impurity phase formed along with CBTO due to the thermodynamic stability of Bi_2WO_6. In addition, CBTO growth was hindered at elevated temperatures (> 600 °C) where Bi_2WO_6 becomes the dominant product. Hence, there is still a need for improving the synthesis protocol to decrease the amount of impurity and effectively evaluate the potential of pure CBTO in photocatalytic reactions. While our previous synthesis approach utilized Cu_2O as the Cu(I) source, an alternative synthetic route for CBTO was described by Kruger and Muller-Buschbaum in 1992, which utilizes Cu_2WO_4 as the Cu(I) source.[12] They generated single crystals of CBTO at 950 °C with this ternary oxide precursor in a heterogenous product mixture of other phases. In the present study, this alternative CBTO synthesis is revisited with some modifications. Unlike the previously-used Cu_2O precursor, which has a tendency to reduce or disproportionate to Cu and result in a loss of Cu by diffusion, as reported in our previous work,[2] the new synthesis employs Cu_2WO_4, in which the association of oxo moieties with tungstate groups decreases the propensity of this precursor to reduce or disproportionate, leading to better retention of Cu in the desired stoichiometric quantity and more predictable synthetic chemistry. With the optimized process, contrary to the earlier work, CBTO can be produced at higher temperatures (up to 800 °C) with much less Bi_2WO_6 phase appearing. Another advantage of the new process is the considerable decrease in synthesis time. In addition, we have characterized photocatalytic properties of CBTO using Cr(VI) reduction

[a] Department of Mechanical and Materials Engineering, Worcester Polytechnic Institute, Worcester, Massachusetts, 01609, USA
[b] Department of Physics, Worcester Polytechnic Institute, Worcester, Massachusetts, 01609, USA
[c] Soldier Protection Directorate, US Army Combat Capabilities Development Command Soldier Center, Natick, Massachusetts, 01760, USA
*Corresponding Author: E-mail address: pmrao@wpi.edu (Pratap M. Rao)
†Electronic Supplementary Information (ESI) available: Details of the characterization techniques, synthesis, and characterization of precursor oxides, additional photocatalysis data. See DOI: 10.1039/x0xx00000x

reaction as a probe and as an environmentally-relevant process. This is the first demonstration of any application of CBTO as a functional material.

Chromium is reported to be the second most abundant inorganic contaminant in the United States and present in drinking water in all states.[13,14] Hexavalent Cr(VI) is a highly toxic (carcinogenic and mutagenic) metal threatening human health and aquatic life seriously even at trace amounts, and has been listed among the 8 highly toxic metals in the US Resource Conservation and Recovery Act.[15–17] Hence removal of Cr(VI) from drinking water is extremely important and urgent. To date, the best remediation strategy has been reduction to less toxic, insoluble Cr(III) species. In this regard, photocatalytic Cr(VI) reduction is attracting interest as an eco-friendly, sustainable, energy saving, fast and cheap technology. With excellent band gap for visible light absorption (E_g ≈ 1.9-2.0 eV) and a conduction band energy (CB) of ~ -0.69 eV (vs. NHE), p-type CBTO is envisioned to be effective in Cr(VI) photoreduction ($E_{Cr(VI)/Cr(III)} = 1.33\ eV\ vs\ NHE$) (Fig. 1). On the other hand, while the valence band (VB) energy of ~ 1.3 eV (vs. NHE) may not be suitable for one electron water oxidation ($E_{\bullet OH/H_2O} = 2.73\ eV\ vs\ NHE$) and/or hydroxyl ion oxidation ($E_{OH^-/\bullet OH} = 1.99\ eV\ vs\ NHE$); the oxidation half-reaction can occur by four electron oxidation of water ($E_{O_2/H_2O} = 1.23\ eV\ vs\ NHE$) and/or oxidation of organic acids, which are typically present in wastewater, or are added for the purpose of this photocatalytic remediation. In this paper, we report photocatalytic activity of CBTO for Cr(VI) reduction and the influence of catalyst loading, pH, and presence of organic acids on the photocatalytic reduction activity. Through the determination of the major active species involved in the photocatalytic processes; we establish the mechanism for the relevant photoreduction/oxidation reactions.

To gain additional insight into the behaviour of the photoexcited carriers, we applied transient absorption spectroscopy (TAS). TAS is a pump-probe technique for characterizing the transient changes in the optical absorption spectrum following the photoexcitation. The decay kinetics of the photogenerated charge carriers can be studied by monitoring these transient changes to understand the timescales of the charge recombination and trapping processes. Here, we report the time-resolved absorption characteristics of CBTO for the first time and discuss the ultrafast dynamics of the photogenerated charge carriers.

2. Experimental

2.1 Materials

All reagents were used as received without further purification unless stated otherwise. Argon (Industrial Grade, 99.995%, Praxair & Ultrapure Grade, 99.999% Airgas) was used for all tube-furnace calcinations. Copper foil (99.9%, 0.254 mm & 0.127 mm thick) and tert-butyl alcohol (TBA, ACS, 99+) were purchased from Alfa Aesar. Copper metal powder (99.999% trace metals basis), copper (II) oxide (CuO, 99.999% trace metals basis), tungsten (VI) oxide (WO_3, 99.995% trace metals basis), bismuth (III) oxide (Bi_2O_3, 99.999% trace metals basis), citric acid (CA, ACS reagent, ≥99.5%), 1,5-Diphenylcarbazide (DPC, reagent Ph. Eur., ≥98.0%), silver nitrate (ACS reagent, ≥99.0%), and p-benzoquinone (BQ, reagent grade., ≥98.0%) were purchased from Sigma Aldrich. Ethanol (absolute, 200 proof, 99.5%, ACS Reagent Grade) was purchased from Acros Organics. Saturated potassium chloride was purchased from VWR. Sulfuric acid (Certified ACS Plus), nitric acid (ACS certified), sodium hydroxide (ACS Certified), and acetone (HPLC Grade) were purchased from Fisher Scientific. Deionized water was generated using a Hydro Service and Supplies water deionizer. Coors high-alumina combustion boats (5mL) and crucibles were purchased from Sigma Aldrich. Sonication treatments were performed in a Branson Bransonics 1800 sonicator. Agate jar and balls for the ball-milling of powders were purchased from MicroNano Tools/Micromolding Solutions Inc. and were used with a PBM-04 Platenary Ball Mill. A Lindberg Blue M box furnace and Lindberg Blue M Mini-Mite one-zone tube furnace from Thermo Scientific were used for solid-state syntheses.

2.2 Synthesis of CBTO

To realize Cu_2WO_4 based synthesis of CBTO, Cu_2WO_4 was freshly prepared by a 2 -step solid-state route as depicted in Fig. 2. Please see ESI for the details of the synthesis and characterization of the precursor (Fig. S1-2). For CBTO synthesis, Cu_2WO_4 (0.5 mmol), Bi_2O_3 (0.5 mmol), and WO_3 (1.5 mmol) were ground to a uniform pinkish-yellow powder by mortar and pestle. The powder mixture was transferred into a folded box of copper foil which was then purged with argon for 10-15 minutes before being folded closed with pliers and placed in a high-alumina combustion boat. The boat was thermally treated at 600 °C (9 hours), 700 °C (30 minutes and 2.5 hours), or 800 °C (10 minutes, 30 minutes, 2 hours, 4 hours and 6 hours) under an argon atmosphere (300 cc/min) in a one-zone tube furnace. The resulting loose crystalline dark red-brown powder was collected from the copper box by opening the box, inverting it, and tapping (Fig. S3a), while any well-adhered material that was deposited on the inner surface of the box was left behind to minimize contamination with copper metal. The dark coloured crystals were powdered by grinding with an agate mortar and pestle before structural characterizations. Post synthesis, ~700 mg of CBTO powder was pre-ground by mortar and pestle for 5 minutes and suspended in ~40 mL ethanol. The suspension was ball-milled for 12 hours at 300 rpm, reversing the direction of rotation every two hours. Following the milling treatment, the powder was collected from the colloidal suspension, dried, and used for the photocatalytic reactions. The ball-milled suspension (without drying) was directly used for drop-casting to prepare films on quartz substrates for transient absorption measurements.

2.2 Characterization

Powder X-ray diffraction (XRD) measurements were performed using a PANalytical Empyrean X-ray diffractometer using Cu K-α (45 kV, 40 mA) and Cr K-α (30 kV, 55 mA) radiation with Ni-β and V-β post-diffracted beam filters, respectively. For consistency all spectra were converted to Cu K-α 2θ values and

reported herein as such. The morphology of the powders was characterized by scanning electron microscopy (SEM, JEOL 7000F, 5kV). All the samples were excited by white light from a 300 W Xe lamp (model 6258, Oriel) and the UV-Vis absorbance spectra were recorded by an Ocean Optics spectrometer (model USB2000+Rad, Ocean Optics). Raman spectroscopy was performed with an excitation laser operating at 532 nm and an Olympus 100× magnification lens. Surface composition of the photocatalyst before and after the photocatalytic reaction was measured by X-ray photoelectron spectroscopy (XPS, Thermo K-Alpha). The transient absorption measurements were obtained by a HARPIA-TA ultrafast transient absorption spectrometer (Light Conversion). The pump-probe signal was generated by a 40 W Ytterbium laser (Carbide, Light Conversion). 450 nm pump pulses with fluence of 76.4 μJ/cm² were generated through an OPA (Orpheus, Light Conversion), and the probe pulses were generated by white light continuum generation through a sapphire crystal. The temporal response was ~150 fs. The pump photon energy of 2.76 eV ensured excitation across the band gap. A white-light continuum between 1.45 and 2.40 eV was used as a probe. The difference in absorption ΔA was detected by an Andor spectrograph and a silicon photodiode, which allowed for detection of the difference in absorption for a single wavelength for every delay time.

2.3 Assessment of photocatalytic Cr(VI) reduction activity

A Cr(VI) stock solution (50 mg /L based on Cr) was prepared by dissolving a suitable amount of $K_2Cr_2O_7$ in deionized water and diluting as needed. To study the photoreduction of Cr(VI) to Cr(III), varying amounts of the photocatalyst (1-16 mg) were added to 40 ml Cr(VI) solution (5 mg/L) at pH 2 (adjusted by adding 1 M HNO_3) containing 10 mM citric acid (CA) in a glass beaker. A VWR SympHony B10P pH meter, which was calibrated daily, was used to measure the pH. Before illumination, the suspension was ultrasonically mixed for 30 min and then magnetically stirred for 30 min in the dark to establish an adsorption–desorption equilibrium between Cr(VI) and the photocatalyst. Afterwards, the test solutions were irradiated by a 300 W Xe lamp fitted with a UV filter under magnetic stirring. Photocatalytic tests were performed under 100 mW/cm² irradiation. At regular intervals, 2 ml of the test solution was withdrawn and centrifuged at 3500 rpm for 10 min to remove the suspended catalyst. The concentration of Cr(VI) in the aqueous solution was determined by measuring the absorption maxima at λ =540 nm using the DPC method.[3,18] The % photoreduction percentage (PRP) was calculated using the following formula:

$$PRP\ (\%) = \frac{A_0 - A_t}{A_0} \times 100 \qquad (1)$$

Where A_0 represents the initial absorbance at time 0 after the treatment in dark, just before light is switched on and A_t is the absorbance after photoreduction process at time t. For determination of the possible reactive species during the photocatalytic reduction, experiments were repeated with TBA, $AgNO_3$, and p-BQ instead of CA to capture hydroxyl radical ($^{\bullet}OH$)[19–21], electrons (e^-)[22], and superoxide radical ($O_2^{\bullet -}$)[18,19,22–26], respectively.

The reusability of CBTO photocatalyst was assessed by performing repeated photocatalytic tests on the same CBTO suspension without any washing or treatment in between runs. For the assessment of the 2nd photocatalytic test, the 1st run with 40 mL of 200 mg/L CBTO suspension with 5 ppm Cr(VI) and 10 mM citric acid was completed without any sampling. After the 1st run, fresh 5 ppm Cr(VI) and 10 mM citric acid were added into the suspension. This suspension was mixed for 60 min. in the darked, followed by illumination with 100 mW/cm² light for the 2nd photocatalytic test. During the 2nd photocatalytic test, 2 mL samples were collected at regular intervals to measure the Cr(VI) concentration. For the assessment of the 3rd photocatalytic test, 1st and 2nd runs were performed as described above without withdrawing any samples during these tests. Before the 3rd test, fresh 5 ppm Cr(VI) and 10 mM citric acid was added into the system. This suspension was mixed for 60 min. in the dark, followed by illumination with 100 mW/cm² light for the 3rd photocatalytic test. During the 3rd photocatalytic test, 2 mL samples were collected at regular intervals to measure the Cr(VI) concentration.

3. Results and discussion

3.1 Improved synthesis of complex oxide CBTO utilizing ternary metal oxide precursor

To test the viability of utilizing a ternary oxide, Cu_2WO_4, as a precursor to CBTO, our earlier reported synthesis protocol (starting with Cu_2O precursor) was reproduced and compared.[2] Selection of the precursor does not significantly impact the synthesis at 600°C. Utilization of the either precursor yields very similar results at this low temperature (Fig. S4), in which there is a persistent BiW_2O_6 impurity even after 4 annealing steps of 9 hours with ball milling between thermal treatments. However, when the temperature is increased to 700 and 800 °C, there is a large difference between the reaction products depending on the precursor used, as can be seen in Fig. 3. Cu_2WO_4-based synthesis yields bulk CBTO as the primary phase even at higher temperatures (700 and 800 °C) and after very short durations. In contrast, Cu_2O-based synthesis results in formation of Bi_2WO_6 as the primary phase and the relative amount of Bi_2WO_6 impurity increases with annealing temperature.

XRD patterns show that with Cu_2WO_4 precursor, bulk CBTO forms after only 10 minutes at 800 °C and after 30 minutes at 700 °C as the primary phase in a sealed Cu box along with secondary impurity phases and the remaining precursors. XRD reflections of the impurity phases and precursors diminish in intensity with longer thermal treatments. The intensity ratio of the most intense reflections for Bi_2WO_6 and CBTO (I_{Bi2WO6}/I_{CBTO}) decreases from 0.64 (1st annealing) to 0.20 (4th annealing) for the Cu_2O-based route (600 °C, 9h). In comparison, the ratio is 0.08 for the Cu_2WO_4-based route after a single, shorter annealing step (800 °C, 4h). The reduction in the amount of the Bi_2WO_6 impurity can be attributed to the

presence of pre-existing Cu-W-O bonds in the Cu_2WO_4 precursor, which minimizes the loss of Cu during synthesis. In addition, utilization of the ternary metal oxide introduces Cu/W sources that are mixed at the atomic level with significantly decreased diffusion distances, which is expected to lower the nucleation barrier to form the solid phase CBTO.[27–29]

Increasing the treatment time further to 6h did not improve the conversion of Bi_2WO_6 to CBTO. Hence, the product prepared using Cu_2WO_4 precursor by the high temperature protocol with lowest fraction of Bi_2WO_6 (Cu_2WO_4 based route, 800 °C, 4h) was selected for further characterization. XRD patterns of different batches show that Cu_2WO_4 based synthesis is a reproducible technique (Fig. S3b).

The morphology and the microstructure of the selected powders were further characterized by SEM. The as-synthesized powder is composed of irregularly shaped particles with well-defined facets (Fig. S5(a,b)). The particle size is highly polydisperse with sizes ranging from ~ 15 µm to 100 nm. To reduce the particle size, the powders were ball-milled before photocatalytic experiments. After the ball-milling, the range of particle sizes was reduced to ~ 2 µm - 20 nm (Fig. S5(c,d)). Energy dispersive X-ray spectroscopy (EDS) analysis of the ball-milled CBTO powder was performed for elemental composition analysis of the synthesized particles. The atomic composition of the larger crystals as well as smaller particles closely resembles that of $CuBiW_2O_8$, with slightly higher Cu than expected, as was found in our previous study (Fig. S6).[2] This slight variation is attributed to the presence of Cu^{2+} on the surface, which was also detected by XPS (Fig. S12) and is likely due to surface oxidation and formation of CuO on the surface. While the powder displays atomic composition ratio similar to that of CBTO, some locations with lower atomic percentage of Cu or Bi than that which would be expected from CBTO were found. This deviation can be attributed to the presence of Bi_2WO_6 and CuW_2O_4 impurity. However, both large and small particles had similar compositions, indicating that the impurity phases are evenly distributed throughout all the particles. XRD patterns of the ball-milled powder are also provided in Fig. S7. All the following characterizations and experiments were performed with the ball milled powder.

3.2 Optical Properties

To evaluate the extent of the visible light absorption, the absorption spectrum of CBTO dispersed in water was recorded (Fig. S8a). CBTO displays strong absorption in the entire visible region extending to the near infrared portion of the spectrum. The Tauc plots obtained from the UV-visible absorption spectrum of CBTO are shown in Fig. 4a. The extrapolated indirect band gap of 1.80 eV is positioned close to the allowed direct band gap of 1.91 eV. These results are in good agreement with previously reported theoretical predictions.[2] The significant lower energy absorption tail covering 1.3 – 1.9 eV range has been previously ascribed to theoretically-predicted intra-valence band absorption associated with the Cu vacancy states, as well as to the absorption by surface states and impurities.

To gain additional insight into the behaviour of the photoexcited carriers, transient absorption spectroscopy (TAS) was performed. TAS spectra at various time delays and the dynamic decay profiles of the associated transitions are given in Fig. 4. The transient differential absorption spectra show an initial broad absorption bleach centered at the direct band gap energy at early times (<10 ps) after excitation (Fig. 4b), resulting from depopulation of the ground state. At early times (<10 ps) bleaching is also observed for intra-band absorption with energy around 1.5 eV. In part, this observed suppression in absorption results from the spectrally broad absorption bleach at 1.9 eV. However, since the energy used in the experiments is sufficient to photoexcite electrons from the deep valence band levels to the top level of the valance band, this short-lived bleach likely also features contributions from state-filling at the top of the valence band (Fig. 4b and c). Then, over short time scales (~10 ps) the free photoexcited electrons and holes are trapped, and therefore both transitions recover (Fig. 4c). The lifetime of these short-lived free carriers is consistent with the lifetime of the free, mobile photoexcited charge carriers determined by optical pump-THz probe (OPTP) spectroscopy in our earlier report[2], which also revealed their mobility to be as high as 150 cm^2/Vs. Most of these free carriers recombine or are trapped at defect or impurity states. The photogenerated electrons may trap at shallow defect states in CBTO, and at Bi_2WO_6 impurities, since the band gap alignment between CBTO and Bi_2WO_6 (Fig. S8b) is favourable for efficient trapping of the photogenerated electrons at the Bi_2WO_6 conduction band. Photogenerated holes, on the other hand, likely trap at the band associated with Cu vacancies in CBTO, which lies within ~0.08 eV of the valence band edge[2]. As a result, not only does the intra-valence band absorption recover, but we also observe the emergence of enhanced broadband photoinduced intra-valence band absorption centered around 1.5 eV, at similar time scales (Fig. 4c). This enhancement of intra-valence band absorption (from states deep in the valence band to states near the top of the valence band) can be explained by the accumulation of a large photogenerated hole concentration near the valance band edge.

Analysis of the longer time dynamics (Fig. 4d) reveals that the trapped photoexcited carriers recombine over ~ 0.5 ns time scales, while relaxation of the photoinduced intra-valence band absorption (1.5 eV) is slower, proceeding with ~ 1.5 ns decay time. These lifetimes are consistent with the nanosecond timescales measured by time-resolved photoluminescence for this population of carriers. The mobility of this long-lived population of trapped carriers was measured by Hall effect to be 0.32 cm^2/Vs, indicating a much slower hopping motion, as expected for trapped carriers.[2]

The new insight obtained here is that the lifetime of these longer-lived slower carriers is of order ~1 ns, resulting in an expected diffusion length of ~30 nm, compared to ~10 nm for the short-lived free carriers. The larger diffusion length of the longer-lived carriers and the good match between this carrier diffusion length and the size of the small ball-milled CBTO particles indicates that these longer-lived carriers in shallow traps are responsible for the majority of the observed

photocatalytic activity. Compared to other multi-metal oxides such as $BiVO_4$ and $CuBi_2O_4$, CBTO exhibits higher carrier mobility and smaller carrier lifetime, but comparable diffusion lengths.[2]

3.3 CBTO as a functional material in photocatalytic applications: Cr(VI) Photoreduction

The photocatalytic behaviour of CBTO was evaluated via photocatalytic Cr(VI) reduction with 10 mM citric acid (CA) present as a hole scavenger under white light excitation from a Xe source with a UV filter (100 mW/cm^2) at pH 2. 400 mg/L of CBTO prepared by Cu_2WO_4-based synthesis (800 °C, 4h) almost completely reduced 5 mg/L Cr(VI) in 15 minutes under these conditions, while the same quantity of CBTO prepared by Cu_2O-based synthesis (600 °C, 9h) required more than 250 minutes to reduce the same quantity of Cr(VI) (Fig. 5a). This difference in performance is in line with our previous assertion[2] that Bi_2WO_6 impurity acts as an efficient trap for the photoexcited carriers in CBTO due to the band offset between these materials (Fig. S8b). Decreasing the amount of Bi_2WO_6 impurity phase using the Cu_2WO_4-based synthesis was crucial to enhance the photocatalytic activity of CBTO. The influence of catalyst loading on dark adsorption of Cr(VI) and on Cr(VI) photoreduction efficiency, and the effect of spectral irradiance on Cr(VI) photoreduction efficiency is given in supporting information (Fig. S9-S10).

We performed experiments with hole and electron scavengers to gain insight into the role of electrons and holes in the photocatalytic process. Addition of an electron scavenger (silver nitrate) decreased the rate of photocatalytic reduction of Cr(VI) (Fig. 5b), while addition of a hole scavenger (citric acid, CA) increased the rate of photocatalytic reduction of Cr(VI) (Fig. 5a-b). This indicates that electrons produced by CBTO directly or indirectly lead to the photoreduction of Cr(VI), while holes provide a competing pathway for consumption of the electrons by recombination. In other words, the improvement in the photoreduction rate of Cr(VI) upon addition of citric acid can be attributed to the enhanced separation of the photoinduced electrons and holes due to the consumption of the photogenerated holes by CA (Fig. 1). The photogenerated electrons and holes are expected to recombine in ~nanoseconds in the absence of CA (Fig. 4b). Hence, CA enhances the availability of the photogenerated electrons to participate in the Cr(VI) photoreduction reactions. However, when the CA concentration exceeds 10 mM, the rate of Cr(VI) photoreduction decreases (Fig. S8a). This decrease is attributed to the reduction of the free surface sites for Cr(VI) adsorption.[30,31] The CA amount was kept constant at 10 mM in the following experiments so as not to hinder the adsorption of Cr(VI) onto the surface. As seen in Fig. S8c, about 88 % of the initial Cr(VI) was adsorbed onto the catalyst surface at the catalyst loading of 400 mg/L even with 10 mM CA present in the solution.

We also performed radical quenching experiments to gain insights into which reaction intermediates are involved in the photocatalytic reduction processes. Specifically, a •OH radical quencher (tert butyl alcohol (TBA)) and a $O_2^{\bullet -}$ radical quencher (p-benzoquinone (BQ)) were added.[18–26] The photoreduction rate of Cr(VI) decreases when each of these radical quenchers is added (Fig. 5b), indicating that both •OH radicals and $O_2^{\bullet -}$ radicals are produced by CBTO and are involved in the photoreduction of Cr(VI). •OH generation through one electron water oxidation ($E^{\bullet OH}/_{H_2O} = 2.73\ eV\ vs\ NHE$)) and/or hydroxyl ion oxidation ($E_{OH^-/\bullet OH} = 1.99\ eV\ vs\ NHE$) are unlikely to be relevant since the valence band (VB) energy of CBTO ($\sim 1.3\ eV\ vs\ NHE$) is not sufficiently positive for these reactions to occur. Another possible pathway is a multistep process through reduction of molecular oxygen to $O_2^{\bullet -}$, disproportionation to H_2O_2 and subsequent reduction to •OH, (possible reactions are listed in Fig. S11) which could also account for the involvement of the superoxide radicals.

The effect of pH on photoreduction of Cr(VI) was also evaluated, as it is an important parameter for actual wastewater treatment. The photoreduction reaction of Cr(VI) proceeds more slowly at neutral pH (Fig. 5a), similar to the previous reports of Cr(VI) photoreduction by other photocatalysts.[18,26,31] This is typically ascribed to the decreased adsorption of Cr(VI) on the catalyst surface due to the less negative charge of the surface at higher pH, and also due to the deposition of $Cr(OH)_3$ precipitate on catalyst surface at high pH values. In this case, the adsorption of the Cr(VI) on CBTO was similar at both acidic (58 %) and neutral pH (55 %) (at 200 mg/L catalyst loading). Hence, the increased rate of Cr(VI photoreduction at low pH can be attributed to the enhanced thermodynamic driving force for Cr(VI) reduction reaction at high [H^+] (Fig. S11).[14] In addition, the acidic conditions hinder the passivation of the catalyst surface by $Cr(OH)_3$ precipitation, thereby enhancing photoreduction of Cr(VI). XPS analysis (Fig. S12) of the catalyst before and after the light induced reactions confirmed the absence of Cr species on the CBTO surface after photoreaction in acidic pH, indicating that reduced Cr product does not coat the photocatalyst under this reaction condition. XPS analysis also shows that features which can be ascribed to surface impurities such as CuO and Bi_2WO_6 are removed during the photocatalytic reaction under the present acidic conditions. On the other hand, features that can be ascribed to CBTO do not show a change in composition after the reaction, which points out the stability of CBTO under photocatalytic reaction conditions. However, a significant reduction in the intensity of the Cu, Bi, and W peaks after the reaction was found, which implies that the surface is coated with some material after the reaction. Analysis of the high resolution C 1s spectra (Fig. S12 and S13) shows that the surface coating is due to carbon species associated with citric acid and/or reduced form of citric acid after the reaction. Some carbon species remain on the surface even after the used catalyst is washed with water and ethanol, but their quantity is greatly reduced, and the Cu, Bi and W peaks from the CBTO surface return to their original intensity after washing.

The reusability of the catalyst was investigated by performing three repeated Cr(VI) photoreduction tests with the same CBTO photocatalyst powder without any treatment or washing of the CBTO in between tests. Prior to the second and third test, the same quantities of Cr(VI) and citric acid that were added for the first test were added into the reactor again. In each test, the suspension was stirred for 60 minutes in the dark to allow

adsorption equilibrium of Cr(VI) and CA with the CBTO particle surface to be reached, followed by illumination to drive the photoreduction of Cr(VI) by CBTO. The fraction of Cr(VI) that was adsorbed on the CBTO surface in the dark (before photoreduction) decreased only slightly in the 2nd and 3rd tests compared to the 1st test. The rate of Cr(VI) photoreduction by CBTO in the 2nd test was nearly identical to that in the 1st test, while the rate in the 3rd test is slightly lower (data shown in Fig. S14). One likely reason for both the slightly lower fraction of dark Cr(VI) adsorption and slightly lower rate of Cr(VI) photoreduction in the 2nd and 3rd tests is that, although the Cr(VI) is almost completely reduced in each test, the CA is not all consumed. Therefore, since the same amount of fresh CA is added in each test, the CA concentration in the 2nd test is higher than in the 1st, and that in the 3rd test is higher than in the 2nd. This results in less adsorption of Cr(VI) and slower photoreduction of Cr(VI) as shown in Fig. S9, because CA competes with Cr(VI) for adsorption onto the CBTO surface. Although we cannot rule out the possibility that deposition of carbon species (derived from CA) on the CBTO surface might also account for some loss in activity, these results suggest that the CBTO photocatalyst does seem to be reusable. Furthermore, a simple calculation suggests that a large number of Cr(VI) ions is photoreducuced in each test relative to the number of surface atoms of CBTO, further supporting the reusability of the CBTO photocatalyst (see ESI for calculation).

As compared to the nanostructured Bi, W and Cu-containing photocatalysts and heterojunction photocatalysts reported in the recent years, CBTO prepared by the improved protocol performs favourably in terms of low catalyst loading, short reaction time to reach 100% Cr(VI) photoreduction for comparable initial Cr(VI) concentration, and low concentration of hole scavenger needed to achieve fast photoreduction (Table S1).[3,16,30–34] In general, the CBTO photocatalyst particles show superior performance compared to other single-material photocatalyst particles, and comparable performance to heterojunction photocatalysts.

4. Conclusions

In conclusion, an improved CBTO synthesis technique overcoming the pitfalls of previously reported protocols was developed. As opposed to a Cu_2O-based synthesis route, utilization of ternary oxide precursor, Cu_2WO_4, facilitates formation of CBTO at higher temperatures in just one thermal treatment step with much shorter time, with much less Bi_2WO_6 impurity. Transient absorption measurements revealed the presence of both short-lived (~10 ps) free photoexcited charge carriers and long-lived (~1 ns) photoexcited charge carriers in shallow traps in the CBTO, with the long-lived carriers having diffusion length of ~30 nm likely being responsible for most of the photocatalytic activity. Experimental data based on Cr(VI) photoreduction established the high photocatalytic activity of the complex oxide CBTO for the first time. The experiments revealed that CBTO can oxidize water and produce superoxide and hydroxyl radicals under visible light irradiation suggesting applicability of CBTO in photocatalytic reactions for water decontamination from organic and inorganic pollutants with visible light. Given the promising Cr(VI) photoreduction ability of CBTO with visible light and the reusability of the CBTO photocatalyst demonstrated through repeated photoreduction tests in this study, it will be valuable to further investigate the interaction between CBTO surface, citric acid, and chromium species to understand and enhance regeneration of the catalyst for longer term real-world applications. Based on the band structure of CBTO, formation of heterojunctions will be beneficial to enhance migration of photogenerated holes away from the VB to facilitate the oxidation half-reaction without the need for hole-scavenging organic acids and to improve the photocatalytic efficiency by increasing electron-hole separation. Furthermore, the CB energy of CBTO is expected to be in the range of -0.6 to -0.7 eV vs NHE, given the measured VB energy (1.31 eV vs NHE) and band gap (1.9-2.0 eV) values. Therefore, the CB and VB of CBTO should straddle the water reduction and oxidation potentials, opening up the possibility that CBTO may be able to achieve overall water splitting (hydrogen and oxygen evolution) if paired with suitable co-catalysts to enhance the kinetics of these reactions, which may be investigated in the future.

Author Contributions

C.Y.A. and J.D. carried out the CBTO synthesis and morpho-structural characterization. E.C.U., and L. V. T. performed the transient absorption measurements and analysed the results. T.L. performed XPS measurements and quantification of the spectra. C.Y.A. carried out photocatalytic reduction tests. C.Y.A., J.D. and P. M. R. conceived the study and wrote the manuscript. All authors discussed the results and commented on the manuscript.

Conflicts of interest

There are no conflicts to declare.

Acknowledgements

This material is based upon work supported by US Army Combat Capabilities Development Command Soldier Center under “Research Collaboration between Worcester Polytechnic Institute (WPI) and CCDC-SC on Advanced Materials”, Project Contract No. W911QY2020001, Public Affairs Office No. PR2022_92549. Authors acknowledge the support of National Science Foundation via the NSF MRI award DMR 2018326. Authors thank Prof. Geoffrey Tompsett for help with the Raman measurements and to Jinzhao Fu and Prof. Yan Wang for their help with the ball milling treatments.

Notes and references

1 M. K. Hossain, E. Kecsenovity, A. Varga, M. Molnár, C. Janáky and K. Rajeshwar, *International Journal of Self-Propagating High-Temperature Synthesis*, 2018, **27**, 129–140.
2 L. Zhou, E. Bainglass, M. Masroor, B. Giri, G. Li, A. Carl, R. L. Grimm, M. N. Huda, L. v. Titova and P. M. Rao, *Journal of Materials Chemistry A*, 2021, **9**, 1643–1654.
3 Q. Yuan, L. Chen, M. Xiong, J. He, S. L. Luo, C. T. Au and S. F. Yin, *Chemical Engineering Journal*, 2014, **255**, 394–402.
4 M. Tayar Galante, A. Živković, J. C. Alvim, C. C. Calchi Kleiner, M. Sangali, S. F. R. Taylor, A. J. Greer, C. Hardacre, K. Rajeshwar, R. Caram, R. Bertazzoli, R. T. Macaluso, N. H. de Leeuw and C. Longo, *ACS Applied Materials and Interfaces*, 2021, **13**, 32865–32875.
5 M. K. Hossain, P. Sotelo, H. P. Sarker, M. T. Galante, A. Kormányos, C. Longo, R. T. Macaluso, M. N. Huda, C. Janáky and K. Rajeshwar, *ACS Applied Energy Materials*, 2019, **2**, 2837–2847.
6 S. P. Berglund, F. F. Abdi, P. Bogdanoff, A. Chemseddine, D. Friedrich and R. van de Krol, *Chemistry of Materials*, 2016, **28**, 4231–4242.
7 S. Pulipaka, N. Boni, G. Ummethala and P. Meduri, *Journal of Catalysis*, 2020, **387**, 17–27.
8 L. Pan, J. H. Kim, M. T. Mayer, M. K. Son, A. Ummadisingu, J. S. Lee, A. Hagfeldt, J. Luo and M. Grätzel, *Nature Catalysis*, 2018, **1**, 412–420.
9 L. Pan, Y. Liu, L. Yao, Dan Ren, K. Sivula, M. Grätzel and A. Hagfeldt, *Nature Communications*, , DOI:10.1038/s41467-019-13987-5.
10 Z. Wu, Z. Zhao, G. Cheung, R. M. Doughty, A. R. Ballestas-Barrientos, B. Hirmez, R. Han, T. Maschmeyer and F. E. Osterloh, *Journal of The Electrochemical Society*, 2019, **166**, H3014–H3019.
11 P. V. Klevtsov and A. P. Perepelitsa, *Zhurnal Neorganicheskoj Khimii*, 2004, **49**, 1021–1025.
12 T. F. Krfiger and H. Mfiller-Buschbaum, *Journal of Alloys and Compounds*, 1992, **190**, L1–L3.
13 A. Vengosh, R. Coyte, J. Karr, J. S. Harkness, A. J. Kondash, L. S. Ruhl, R. B. Merola and G. S. Dywer, *Environmental Science and Technology Letters*, 2016, **3**, 409–414.
14 C. M. Stern, T. O. Jegede, V. A. Hulse and N. Elgrishi, *Chemical Society Reviews*, 2021, 50, 1642–1667.
15 C. Athanasekou, G. E. Romanos, S. K. Papageorgiou, G. K. Manolis, F. Katsaros and P. Falaras, *Chemical Engineering Journal*, 2017, **318**, 171–180.
16 C. He, L. Gu, Z. Xu, H. He, G. Fu, F. Han, B. Huang and X. Pan, *Environmental Chemistry Letters*, 2020, 18, 561–576.
17 *The Resource Conservation and Recovery Act of 1976* , 1976.
18 S. M. Ghoreishian, K. S. Ranjith, B. Park, S. K. Hwang, R. Hosseini, R. Behjatmanesh-Ardakani, S. M. Pourmortazavi, H. U. Lee, B. Son, S. Mirsadeghi, Y. K. Han and Y. S. Huh, *Chemical Engineering Journal*, 2021, **419**, 129530.
19 M. Pelaez, P. Falaras, V. Likodimos, K. O'Shea, A. A. de la Cruz, P. S. M. Dunlop, J. A. Byrne and D. D. Dionysiou, *Journal of Molecular Catalysis A: Chemical*, 2016, **425**, 183–189.
20 Y. Zhiu, Y. Liu, Y. Lv, Q. Ling, D. Liu and Y. Zhu, *Journal of Materials Chemistry A*, 2014, **2**, 13041–13048.
21 X. Zhang, F. Tian, L. Qiu, M. Gao, W. Yang, Y. Liu and Y. Yu, *Journal of Materials Chemistry A*, 2021, **9**, 10297–10303.
22 V. Manikandan, M. A. Mahadik, I. S. Hwang, W. S. Chae, J. Ryu and J. S. Jang, *ACS Omega*, 2021, **6**, 23901–23912.
23 D. Wang, L. Guo, Y. Zhen, L. Yue, G. Xue and F. Fu, *Journal of Materials Chemistry A*, 2014, **2**, 11716–11727.
24 J. Li, J. Wang, J. Liu, Y. Li, H. Ma, J. Yang and Q. Zhang, *RSC Advances*, 2020, **10**, 43193–43203.
25 X. Yuan, X. Wu, Z. Feng, W. Jia, X. Zheng and C. Li, *Catalysts*, , DOI:10.3390/catal9070624.
26 P. Dhiman, S. Sharma, A. Kumar, M. Shekh, G. Sharma and M. Naushad, *Ceramics International*, 2020, **46**, 12255–12268.
27 K. Vidyasagar, J. Gopalakrishnan and C. N. R. Rao, *Inorganic Chemistry*, 1984, **23**, 1206–1210.
28 C. N. R. Rao and J. Gopalakrishnan, *Acc. Chem. Res.*, 1987, **20**, 228–235.
29 H. Lu, D. S. Wright and S. D. Pike, *Chemical Communications*, 2020, **56**, 854–871.
30 D. Majhi, A. Kumar Mishra, K. Das, R. Bariki and B. G. Mishra, *Chemical Engineering Journal*, 2021, **413**, 1227506.
31 Q. Xu, R. Li, C. Wang and D. Yuan, *Journal of Alloys and Compounds*, 2017, **723**, 441–447.
32 M. Kebir, A. Boudjemaa, Y. Azoudj, M. Sehailia and K. Bachari, *Canadian Journal of Chemical Engineering*, 2018, **96**, 2292–2298.
33 F. Xu, H. Chen, C. Xu, D. Wu, Z. Gao, Q. Zhang and K. Jiang, *Journal of Colloid and Interface Science*, 2018, **525**, 97–106.
34 L. Shi, Z. Li, K. Marcus, G. Wang, K. Liang, W. Niu and Y. Yang, *Chemical Communications*, 2018, **54**, 3747–3750.

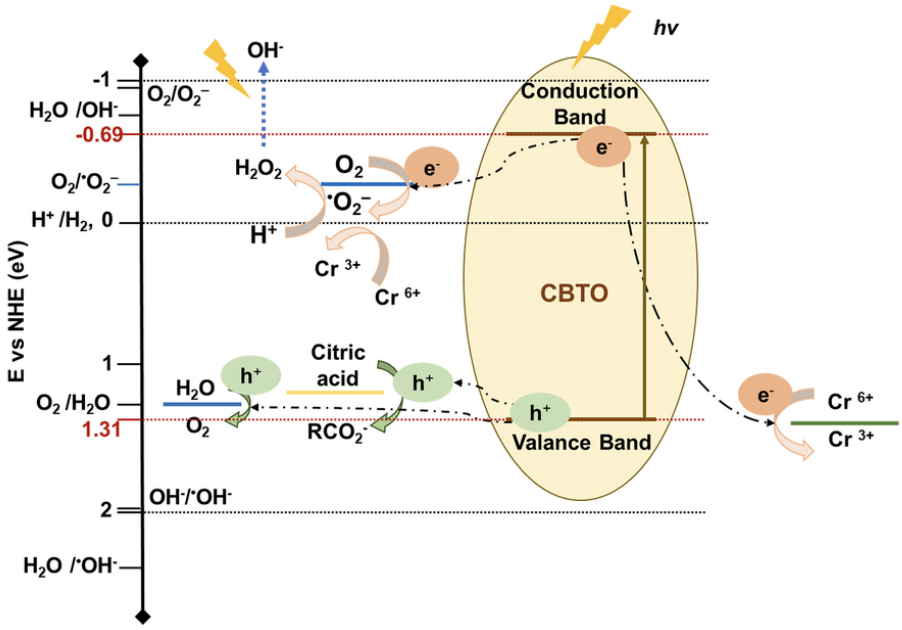

Fig.1 Schematic illustration of the CBTO band structure, photoinduced charge carrier separation, and the photocatalytic Cr(VI) reduction reaction mechanism

82x53mm (300 x 300 DPI)

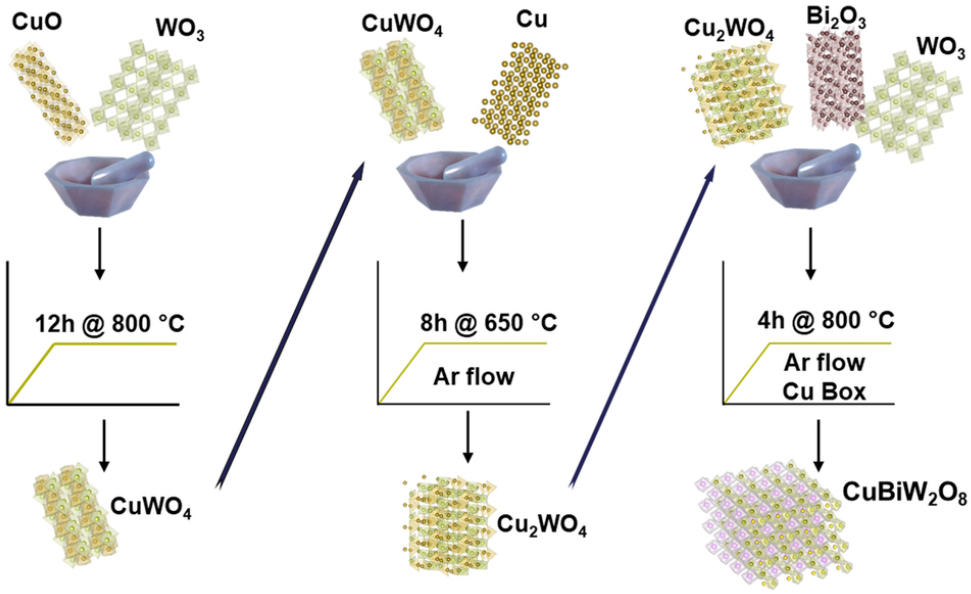

Fig.2 Scheme summarizing the optimized synthetic protocols (VESTA was used for crystal structure visualization)

82x50mm (300 x 300 DPI)

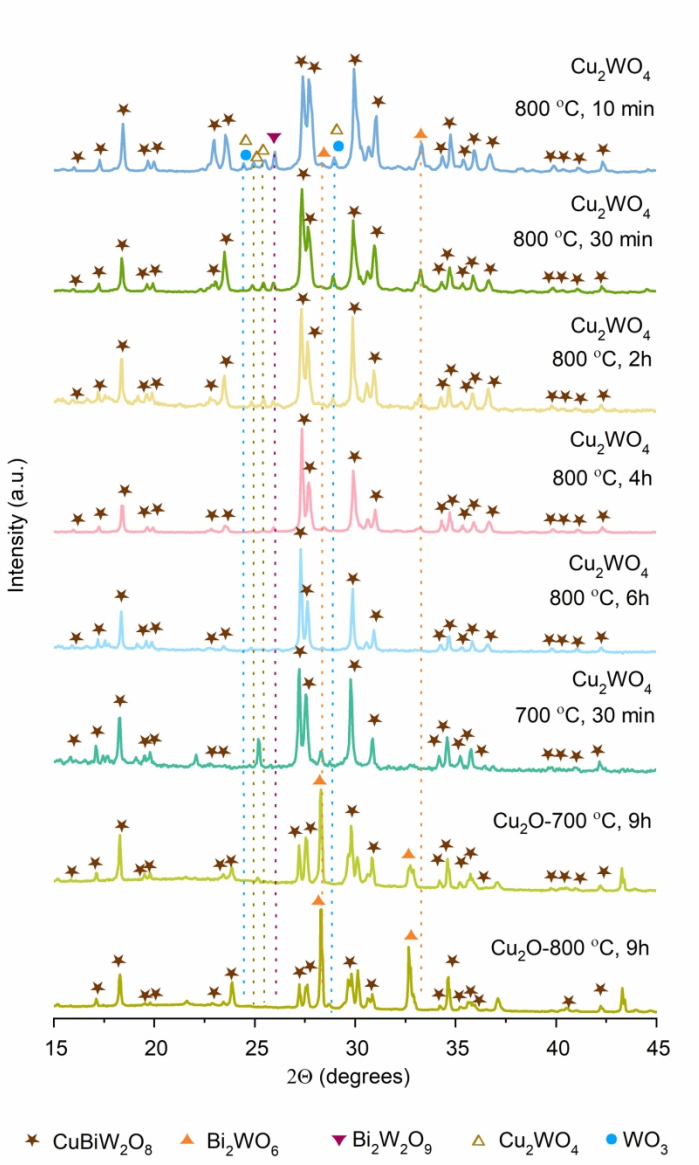

Fig.3 XRD diagrams showing Cu_2WO_4 based CBTO synthesis at varying temperatures and durations in Cu rich environment under Argon compared with Cu_2O based synthesis

70x120mm (600 x 600 DPI)

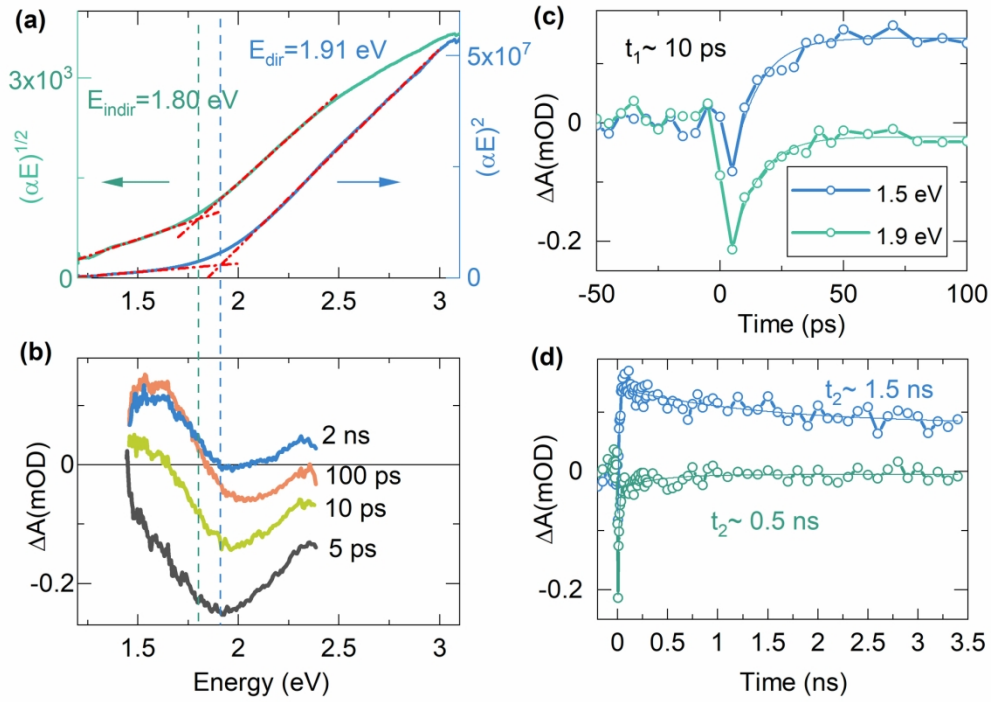

Fig.4 Optical properties of CBTO (a) Tauc plot for determining the indirect (1.80 eV) and direct (1.91 eV) band gaps. (b) Transient absorption spectra recorded at different times after excitation with 76.4 μJ/cm2, 450 nm (2.76 eV) optical pulses. Transient absorption kinetics at 1.5 eV and 1.9 eV over early (c) and long (d) time scales.

82x59mm (600 x 600 DPI)

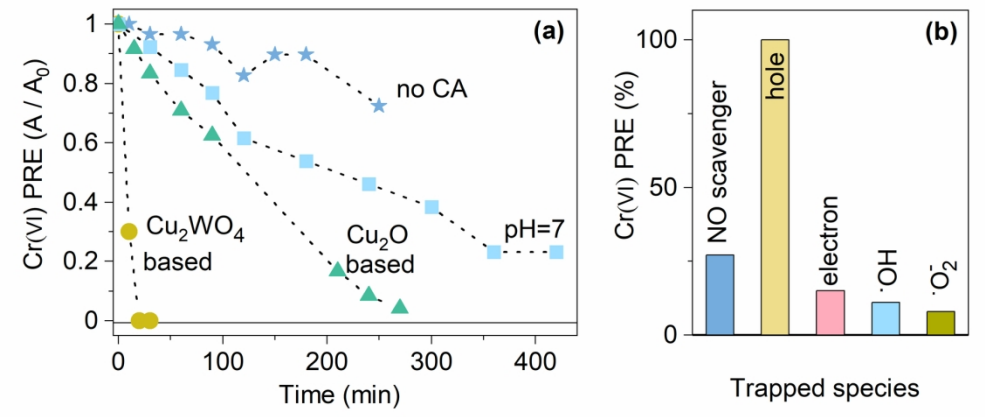

Fig.5 Cr(VI) photoreduction with CBTO under excitation with 100 mW/cm^2 light , 40 ml of 5 mg/L Cr(VI) solution, 10 mM CA, pH=2 unless stated otherwise (a) depending on synthesis technique, pH, and (b) presence of citric acid PRP at 240 min. in the presence of different scavengers (CBTO: 200 mg/L)

82x34mm (600 x 600 DPI)